Solid State Communications 150 (2010) 1760–1765

Contents lists available at ScienceDirect

Solid State Communications

journal homepage: www.elsevier.com/locate/ssc

Quasiperiodic magnonic superlattices with mirror symmetry

I.P. Coelho [a,c], M.S. Vasconcelos [b,*], C.G. Bezerra [c]

[a] Departamento de Ensino Superior, Instituto Federal de Educação, Ciência e Tecnologia do Maranhão, Imperatriz-MA 65919-050, Brazil

[b] Escola de Ciências e Tecnologia, Universidade Federal do Rio Grande do Norte, Natal-RN 59072-970, Brazil

[c] Departamento de Física, Universidade Federal do Rio Grande do Norte, Natal-RN 59072-970, Brazil

ARTICLE INFO

Article history:
Received 1 June 2010
Received in revised form
9 July 2010
Accepted 12 July 2010
by A.H. MacDonald
Available online 18 July 2010

Keywords:
A. Metamagnetic materials
A. Magnonic superlattices
C. Quasicrystals
D. Spin waves

ABSTRACT

We address the spin wave modes propagating in Fibonacci, Thue–Morse, and double period quasiperiodic magnonic superlattices. These structures are made of layers of a metamagnetic material alternating with layers of a nonmagnetic material, presenting mirror symmetry. Our calculations are carried out in the magnetostatic regime for the antiferromagnetic phase. Our model takes into account the presence of an external applied magnetic field, which is perpendicular to the interfaces of the superlattice, as well as the crystalline anisotropic contribution to the inner magnetic field. The magnetostatic bulk and surface modes are obtained by using the transfer matrix technique. The metamagnetic material considered here is $FeBr_2$, however, our results can be extended to other materials. Our numerical results show the behavior of these modes, for small frequencies of the energy spectra. The results reported here can be experimentally observed by light scattering techniques.

1. Introduction

The importance of quasiperiodic structures can be estimated by the large bibliography published about this subject in the past decades [1,2]. A quite interesting characteristic of these quasiperiodic crystals is the fact that they display collective properties, due to the presence of long-range correlations, that are not shared by their constituents. On the one hand, from a theoretical perspective, quasiperiodic systems present a variety of interesting features such as, fractal spectra, scaling laws, localization of states, oscillatory specific heat [3], etc. Besides, apart from their theoretical relevance, they have technological potential in several areas.

On the other hand, from a experimental perspective, the advances in experimental growth techniques made it possible to synthesize multilayers and superlattices of impressive quality, for instance by means of "sputtering" and molecular beam epitaxy. In particular, layered magnetic systems have been attractive objects of research in the past years because of the discovery of physical properties such as giant magnetoresistance [4], large out-of-plane magnetic anisotropy [5], resonant absorption of microwaves [6], and magnetic field controlled photonic band gaps [7], etc. As a consequence, layered magnetic systems have became promising for technological applications, particularly as magnetic sensors and memories of random access [8]. As a matter of fact, very recently, Fibonacci quasiperiodic Fe/Cr multilayers were grown on MgO (100) using dc magnetron sputtering [9].

A very interesting example of magnetic system is the so-called metamagnetic material. It is a system presenting a hexagonal structure whose spins, within a specific layer, are ferromagnetically coupled, while the spins in adjacent layers are antiferromagnetically coupled. It should be remarked that the ferromagnetic intralayer exchange interaction is much stronger than the weak antiferromagnetic interlayer exchange interaction between adjacent layers [10]. In the regime of low temperatures, for small values of the external magnetic field H_0, the adjacent layers of the metamagnetic material are antiparallel to each other, giving rise to the antiferromagnetic phase (AFM). Moreover, for H_0 large enough to overcome the interlayer antiferromagnetic coupling, the overall ordering is ferromagnetic, characterizing the ferromagnetic phase (FM).

In recent years, since the pioneering work of Yablonovitch [11] and John [12], considerable effort has been also made in dielectric microstructures with modulated periodicity that exhibit unique properties as *photonic band gaps*, i.e., photonic crystals. The concept of photonic band gaps is quite similar to the one corresponding to electrons in solid state physics: the propagation of photons is forbidden in photonic band gaps. Moreover, it is possible to create similar crystals for which, instead of electromagnetic waves, spin waves (SW) are used as the carriers of information. Drawing an analogy from photonic and phononic crystals, they may be called *magnonic crystals* (MC) (because magnons are the quasiparticles of SW). Therefore, it is also possible to manipulate

* Corresponding author. Tel.: +55 84 3344 3823; fax: +55 84 3344 3821.
E-mail addresses: isaias@dfte.ufrn.br (I.P. Coelho), mvasconcelos@yahoo.com.br, manoelvasconcelos@yahoo.com.br (M.S. Vasconcelos), cbezerra@dfte.ufrn.br (C.G. Bezerra).

0038-1098/$ – see front matter © 2010 Elsevier Ltd. All rights reserved.
doi:10.1016/j.ssc.2010.07.023

magnons in microstructures in a similar way in which electrons are manipulated in semiconductor crystals [13–15]. As a consequence, many potential applications may emerge from the physical properties of MC. For example, recently it has been shown that the spectrum of MC is strongly influenced by the presence of *magnonic band gaps* in which magnon propagation is forbidden [15]. In this work we calculate the forbidden and allowed magnonic band gaps for quasiperiodic metamagnetic magnonic superlattices with mirror symmetry. This work is organized as follows. In Section 2 we present the general theory to describe the magnetostatic modes. Section 3 is devoted to describing the stacking pattern of the system, as well as the transfer matrix technique. Finally, in Section 4 our numerical results and conclusions are presented.

2. General theory

We present the general model to describe the magnon dispersion relation in the magnetostatic regime, which can propagate in a semi-infinite metamagnetic magnonic superlattice with mirror symmetry. Although the model is already described elsewhere, we prefer to describe it again, for the reader's convenience, following the lines of Ref. [16].

In the magnetostatic limit, Maxwell's equations can be expressed as

$$\vec{\nabla}.\vec{B} = 0, \qquad \vec{\nabla} \times \vec{h} = 0, \tag{1}$$

and with the constitutive tensorial relation $\vec{B} = \mu\vec{h}$, where μ is the permeability tensor. The geometry used here is shown in Fig. 1, where we consider that $\vec{M}$ (the saturation magnetization) and $\vec{H}_0$ (the external magnetic field) are perpendicular to the superlattice interfaces. Considering that the external field presents a time dependence of the form $\exp(-i\omega t)$, the permeability tensor can be evaluated and it is given by [16]

$$\mu = \begin{bmatrix} \mu_1 & i\mu_2 & 0 \\ -i\mu_2 & \mu_1 & 0 \\ 0 & 0 & 1 \end{bmatrix}, \tag{2}$$

with

$$\mu_1 = 1 + \frac{4\pi(A_1\omega^2 + B_1)}{(\omega^2 - \omega_1)(\omega^2 - \omega_2)}, \tag{3}$$

and

$$\mu_2 = \frac{4\pi(A_2\omega^3 + B_2\omega)}{(\omega^2 - \omega_1)(\omega^2 - \omega_2)}. \tag{4}$$

Here

$$A_1 = (\omega_{Mii} + \omega_{Mjj})(\omega_1 + \omega_2) + b, \tag{5}$$

$$A_2 = \omega_{Mii} + \omega_{Mjj}, \tag{6}$$

$$B_1 = b\omega_1\omega_2, \tag{7}$$

$$B_2 = (\omega_{Mii} + \omega_{Mjj})\omega_1\omega_2 + b(\omega_1 + \omega_2), \tag{8}$$

and

$$b = \omega_{Mii}(\omega_{ji} - \omega_{jj}) + \omega_{Mjj}(\omega_{ij} - \omega_{ii}). \tag{9}$$

Finally, the relations

$$\omega_{1,2} = -(1/2)(\omega_{ij} + \omega_{ji}) \pm (1/2)[(\omega_{ij} - \omega_{ji})^2 + 4\omega_{ii}\omega_{jj}]^{1/2} \tag{10}$$

define two resonance frequencies of the metamagnetic material. The upper (lower) sign refers to ω_1 (ω_2). The first resonance frequency ω_1 is related to the precession of the magnetization, $\vec{M} = \vec{M}_i + \vec{M}_j$, around the effective static field, which defines the ferromagnetic phase. The second resonance frequency ω_2 is related to the precession of the magnetization around the exchange field H_E, which defines the antiferromagnetic phase. More specifically,

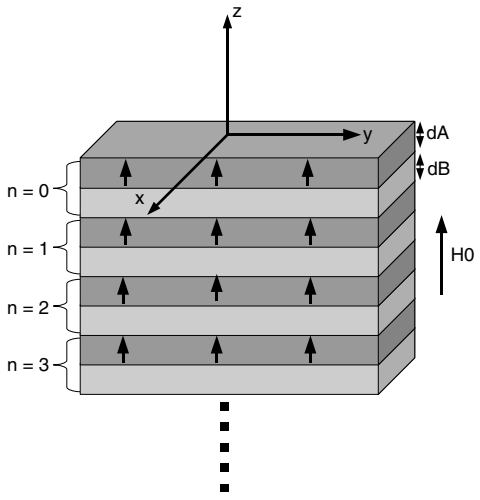

Fig. 1. The geometry of the magnonic superlattice used in this paper. The thickness of the magnetic layer is d_A and the thickness of the nonmagnetic layer is d_B. The length of the unit cell is $L = d_A + d_B$ and unit cells are indexed by n.

the frequencies in the above equations are given by [16]

$$\gamma^{-1}\omega_{ij} = -H_E - H_A - H_0 + (1/3)M_j^z, \tag{11}$$

$$\gamma^{-1}\omega_{ji} = H_E + H_A - H_0 - (1/3)M_i^z, \tag{12}$$

$$\gamma^{-1}\omega_{\eta\eta} = \mp H_E \pm (1/3)M_\eta^z, \tag{13}$$

and

$$\gamma^{-1}\omega_{M\eta\eta} = \mp M_\eta^z. \tag{14}$$

Here η means i or j, with the upper (lower) sign related to i (j).

It is known that we can define the magnetic scalar potential ψ from Eq. (1) (since $\vec{h} = -\nabla\psi$). We use the constitutive tensorial relation $\vec{B} = \mu\vec{h}$ to obtain

$$\mu_1\left(\frac{\partial^2\psi}{\partial x^2} + \frac{\partial^2\psi}{\partial y^2}\right) + \frac{\partial^2\psi}{\partial z^2} = 0. \tag{15}$$

In order to find the bulk magnetostatic modes, we apply the solution of Eq. (15) at the interfaces of the magnonic superlattice, taking into account the following boundary conditions: ψ and $\partial\psi/\partial z$ have to be continuous across the interfaces. We can assume plane wave solutions,

$$\psi = \psi(z)\exp(i\vec{k}_\parallel \cdot \vec{\rho}_\parallel - \omega t). \tag{16}$$

Here $\vec{k}_\parallel$ and $\vec{\rho}_\parallel$ are the in-plane wavevector and position vector, respectively. Applying (16) in Eq. (15), and considering $|\vec{k}_\parallel| = k$, one gets

$$\left(-\mu_1 k^2 + \frac{d^2}{dz^2}\right)\psi = 0, \tag{17}$$

whose solutions are of the type $\psi(z) = Ae^{\alpha z} + Be^{-\alpha z}$, where $\alpha = (\mu_1)^{1/2}k$. Note that for frequencies and wavevectors such that $\mu_1 < 0$, we have oscillatory solutions for $\psi(z)$. It can be shown that $\mu_1 < 0$ is a sufficient condition in order to obtain the bulk and surface modes [17].

3. Magnonic superlattice structure

We consider the quasiperiodic magnonic superlattice composed of layers of a metamagnetic material A alternating with layers of a nonmagnetic material B, as is depicted in Fig. 1. They are stacked in a quasiperiodic array of Fibonacci, Thue–Morse and double period type with mirror symmetry (see description later in this section). The thickness of each material is d_A and d_B, respectively.

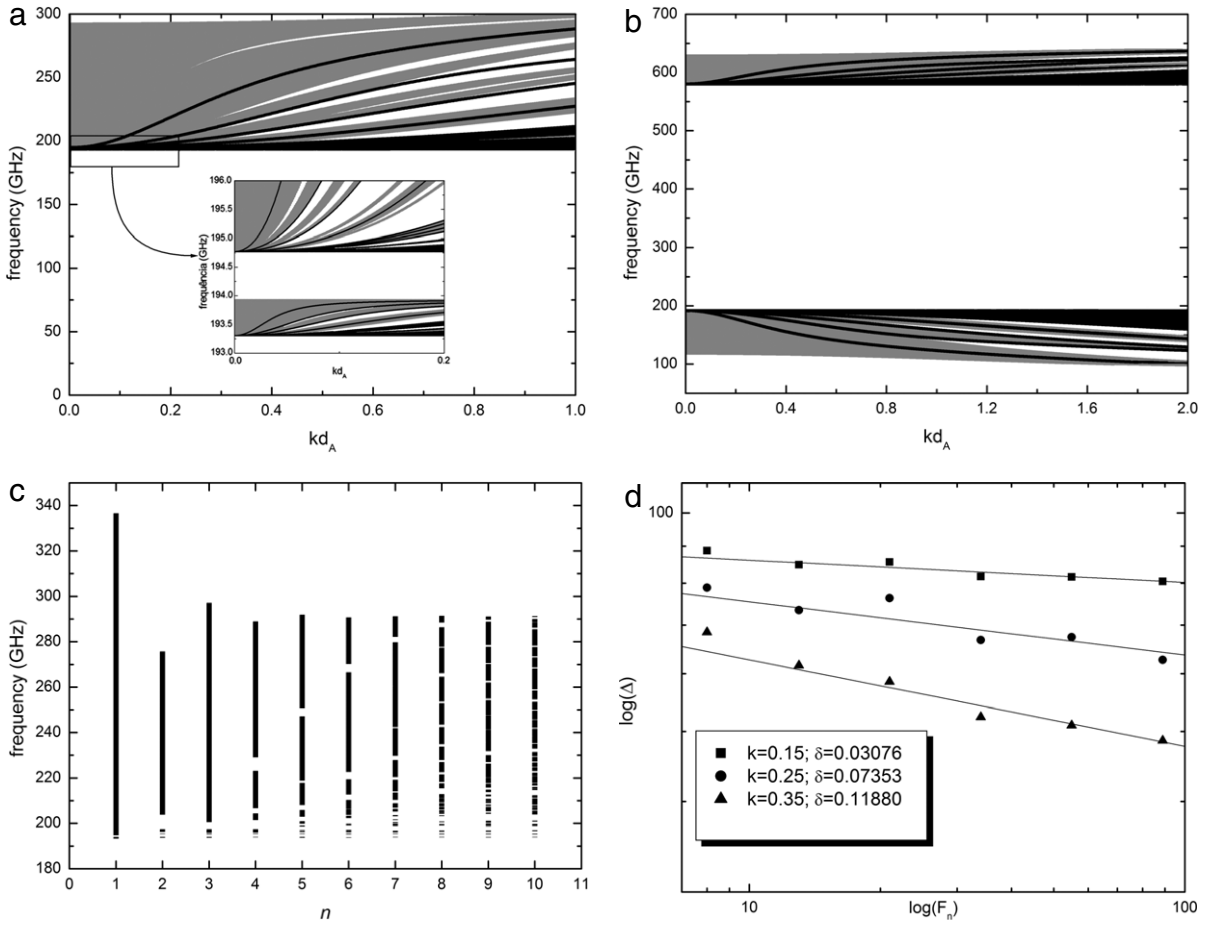

Fig. 2. (a) Spin wave dispersion relation for the fifth generation of the Fibonacci sequence with $H_0 = 0$. The shaded regions and thin lines correspond to bulk and surface modes, respectively; (b) the same as (a), but for $H_0 = 22$ kG; (c) the distribution of bandwidths as a function of the Fibonacci generation index N; (d) log–log plot of the total allowed bandwidth Δ versus the Fibonacci number F_N.

We assume that within the bulk of each material the magnetic scalar potential has the form

$$\psi(z) = A_+ e^{\alpha z} + A_- e^{-\alpha z} \tag{18}$$

for the magnetic layer, and

$$\psi(z) = B_+ e^{kz} + B_- e^{-kz} \tag{19}$$

for the nonmagnetic layer. We apply the boundary conditions at the interfaces $z = nL + d_A$ and $z = (n+1)L$, where n is the unit cell index (see Fig. 1). After a long but straightforward calculation, we obtain

$$|A^{n+1}\rangle = T|A^n\rangle. \tag{20}$$

Here T is the transfer matrix of the system. It connects the amplitudes of the magnetic scalar potential of two consecutive unit cells. Therefore, $|A^n\rangle$ and $|A^{n+1}\rangle$ are column vectors corresponding to the amplitudes of the magnetic scalar potential of the nth and $(n+1)$th unit cells, respectively. The explicit form of the transfer matrix T can be found elsewhere (see Ref. [18]). Using Eq. (20) together with Bloch's theorem it is easy to show that the implicit dispersion relation for the magnetostatic bulk modes is of the form $\cos(QL) = \frac{1}{2}\mathrm{Tr}[T]$, where Q is the Bloch wavevector.

To analyze the surface modes, we consider the truncation of the superlattice at the plane $z = 0$, so that we now have a semi-infinite magnonic superlattice occupying the region $z < 0$. For this case Bloch's theorem still holds provided we replace the Bloch wavevector Q by $i\beta$, with $Re(\beta) > 0$ to guarantee a localized mode. The implicit dispersion relation for the surface modes is given by $T_{11} + \lambda T_{12} = T_{22} + \lambda^{-1} T_{21}$, where T_{ij} are the elements of the transfer matrix and $\lambda = (\alpha + k)/(\alpha - k)$.

Once we know the implicit expression for the magnetostatic modes, let us now describe the construction of the quasiperiodic sequences. A Fibonacci sequence with mirror symmetry can be expressed as $S_N = L_N R_N$, where L_N is generated by the inflation rule $A \to AB$ and $B \to A$, while R_N is generated by the inflation rule $A \to BA$ and $B \to A$. Using the inductive method described in Ref. [19], the transfer matrix T_N for a given generation N of the Fibonacci sequence can be written as

$$T_N = \begin{cases} S_N^L S_N & \text{for } N \text{ odd}, \\ N_{AB} S_N^L N_{BA} S_N & \text{for } N \text{ even}, \end{cases} \tag{21}$$

where

$$S_N = S_{N-2} S_{N-1} \quad (N \geq 2) \tag{22}$$

and

$$S_N^L = \begin{cases} N_{AB} S_{N-1}^L N_{BA} S_{N-2}^L & \text{for } N \text{ odd}, \\ N_{BA} S_{N-1}^L N_{AB} S_{N-2}^L & \text{for } N \text{ even}, \end{cases} \quad (N \geq 2) \tag{23}$$

with initial conditions $S_0 = S_0^L = N_B^{-1} M_B$, $S_1 = S_1^L = N_A^{-1} M_A$, $N_{AB} = N_A^{-1} N_B$ and $N_{BA} = N_B^{-1} N_A$. Therefore, we can find the transfer matrix for any generation N (see Ref. [18]).

The Thue–Morse sequence with mirror symmetry can be expressed as $S_N = L_N R_N$, where L_N is generated by the inflation rule $A \to AB$ and $B \to BA$, while R_N is generated by $A \to BA$ and $B \to AB$. For this sequence the transfer matrix T_N is given by

$$T_N = \begin{cases} N_A^{-1} S_{\alpha_N} S_{\beta_N} S_{\beta_N} S_{\alpha_N} N_A & \text{for } N \text{ odd}, \\ N_A^{-1} S_{\beta_N} S_{\alpha_N} S_{\beta_N} S_{\alpha_N} N_A & \text{for } N \text{ even}, \end{cases} \tag{24}$$

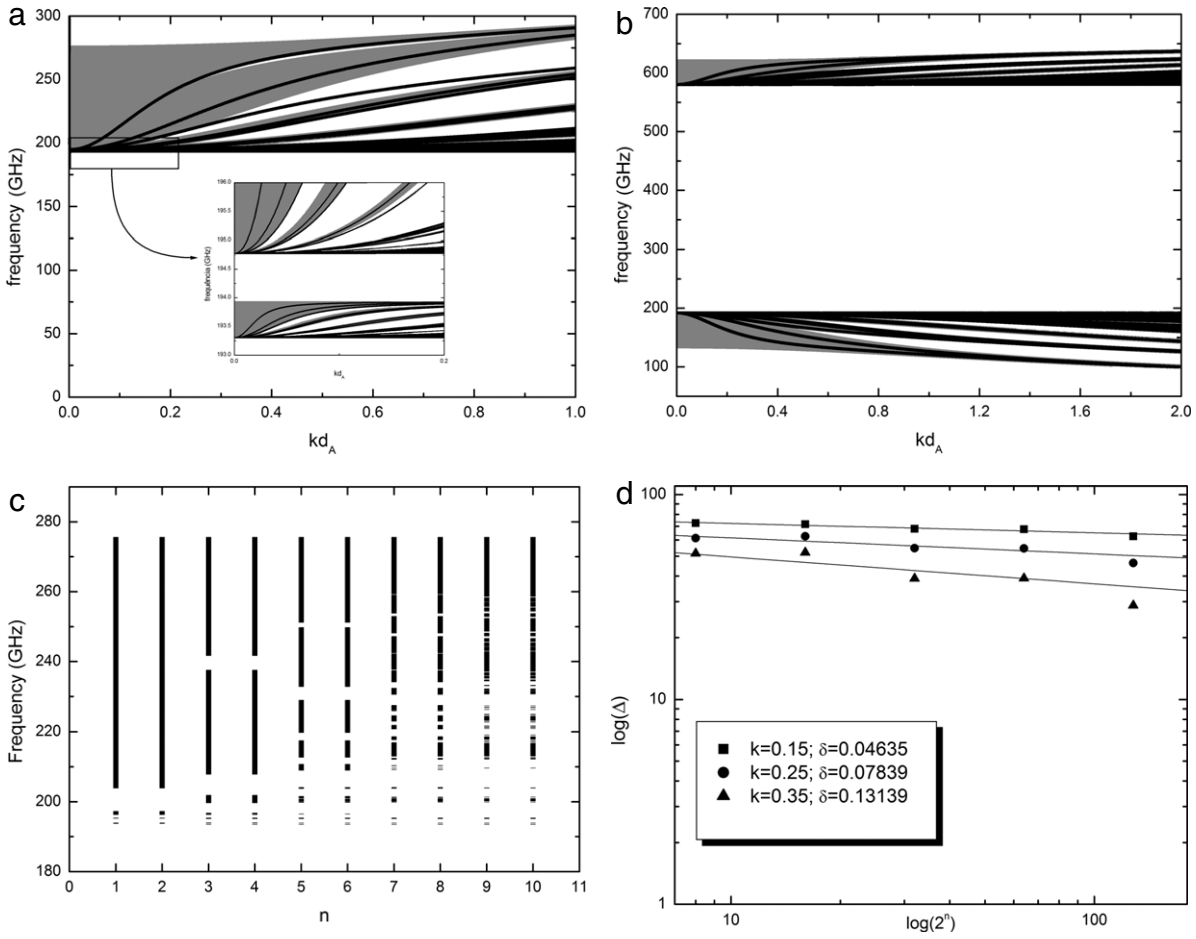

Fig. 3. (a) Spin wave dispersion relation for the fourth generation of the Thue–Morse sequence with $H_0 = 0$. The shaded regions and thin lines correspond to bulk and surface modes, respectively; (b) the same as (a), but for $H_0 = 22$ kG; (c) the distribution of bandwidths as a function of the Thue–Morse generation number N; (d) log–log plot of the total allowed bandwidth Δ versus the Thue–Morse generation number N.

where

$$S_{\alpha_{N+1}} = S_{\beta_N} S_{\alpha_N}, \tag{25}$$

$$S_{\beta_{N+1}} = S_{\alpha_N} S_{\beta_N}, \tag{26}$$

with initial conditions $S_{\alpha_1} = M_A N_A^{-1}$ and $S_{\beta_1} = M_B N_B^{-1}$ (see Ref. [18]).

In a similar way, the double period sequence with mirror symmetry can be represented as $S_N = L_N R_N$, where L_N is generated by an equivalent inflation rule $A \to AB$ and $B \to AA$, while R_N is generated by $A \to BA$ and $B \to AA$. The transfer matrix for the double period case is given by

$$T_N = \begin{cases} N_{AB} S_N^L N_{BA} S_N & \text{for } N \text{ odd}, \\ S_N^L S_N & \text{for } N \text{ even}, \end{cases} \tag{27}$$

where

$$S_N = S_{N-2} S_{N-2} S_{N-1} \quad (N \geq 2) \tag{28}$$

and

$$S_N^L = \begin{cases} N_B^{-1} S_{N-1}^L M_A N_A^{-1} S_{N-1}^L M_B & \text{for } N \text{ odd}, \\ N_A^{-1} S_{N-1}^L M_B N_B^{-1} S_{N-1}^L M_A & \text{for } N \text{ even} \end{cases} \quad (N \geq 1) \tag{29}$$

where the initial conditions are $S_0 = S_0^L = N_A^{-1} M_A$, $S_1 = S_1^L = N_A^{-1} M_B N_B^{-1} M_A$ (see Ref. [18]).

4. Numerical results

Let us now present some numerical results of the spin wave dispersion relation, for the quasiperiodic metamagnetic magnonic superlattices, as a function of the frequency ω versus kd_A. Along this section we will compare our present results with previous results for the periodic metamagnetic magnonic superlattice reported in Ref. [16]. In what follows, the values of the physical parameters used (exchange and anisotropy fields) are known by Raman scattering experiments [20]: $J = 5.07$ cm^{-1}, $\gamma H_A = 7.34$ kG, $\gamma M_i^z = 1.2$ kG, $\gamma M_j^z = 1.45$ kG, and $d_A = d_B = 100$ nm. We considered $FeBr_2$ in its AFM phase, spin $S = 1$ and critical temperature $T_c = 14.2$ K. In all figures, the bulk bands are shown shaded and they are limited by the curves $QL = 0$ and $QL = \pi$. In between these curves there are gap regions where the surface modes can propagate.

Fig. 2(a) shows the magnon spectra for the fifth generation of the Fibonacci sequence with mirror symmetry. In contrast with the periodic case for which there exists a large band gap between high- and low-frequency modes for $H_0 = 0$ [16], the inset shows that the modes are closing into two regions, as expected due to the antiferromagnetic phase at $H_0 = 0$. The modes are concentrated in the high-frequency region. The high-frequency branch is in the range 194.8 GHz $< \omega <$ 290.9 GHz, while the low-frequency branch is in the range 193.3 GHz $< \omega <$ 193.9 GHz (for zero external applied field and $kd_A = 0$). The behavior found in both regions is already expected (see for example Camley and Cottam [17]). The spectra with an external applied field of $H_0 = 22$ kG is illustrated in Fig. 2(b). One can observe (i) a narrowing of the allowed frequency regions and (ii) the modes are now concentrated in the low-frequency region. A quite similar behavior occurs for the periodic case; however the forbidden regions are larger than for the

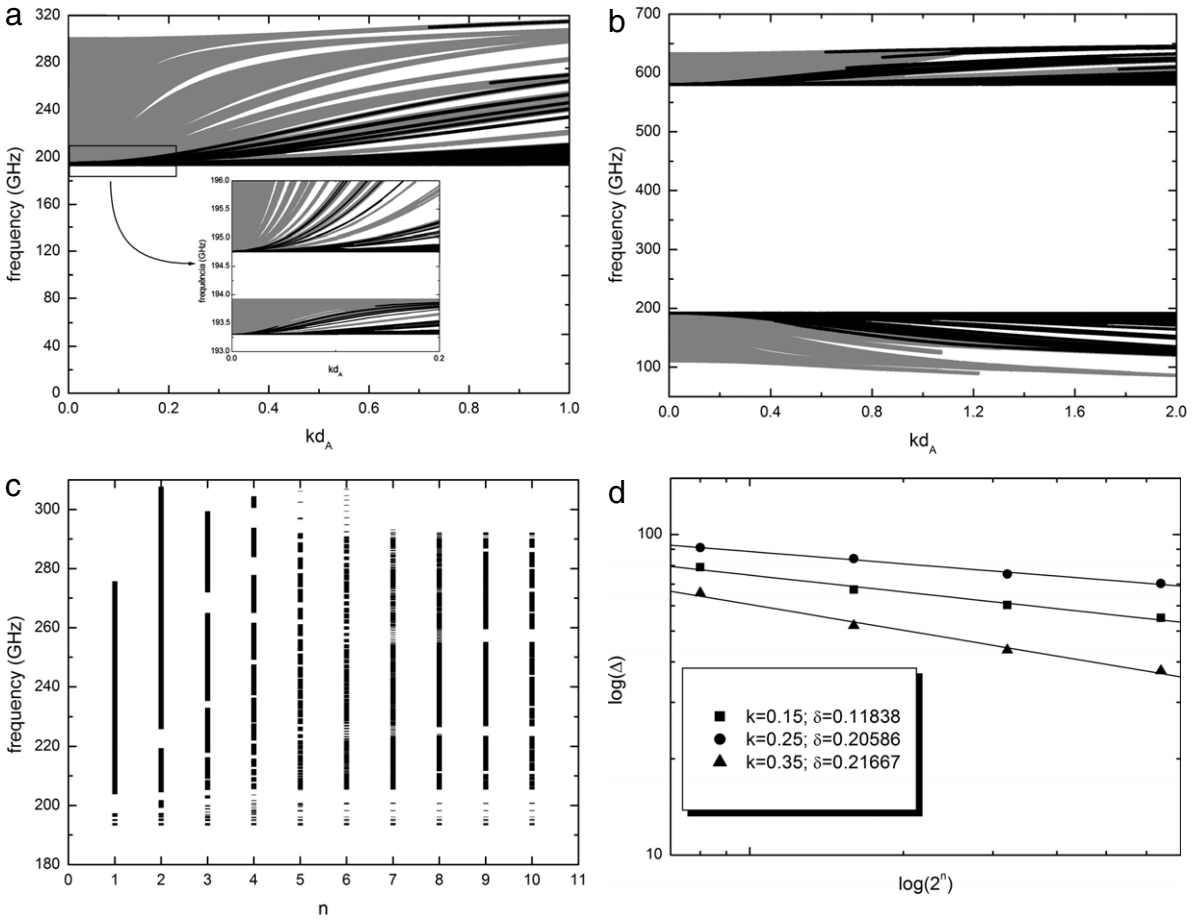

Fig. 4. (a) Spin wave dispersion relation for the fourth generation of the double period sequence with $H_0 = 0$. The shaded regions and thin lines correspond to bulk and surface modes, respectively; (b) the same as (a), but for $H_0 = 22$ kG; (c) the distribution of bandwidths as a function of the double period generation number N; (d) log–log plot of the total allowed bandwidth Δ versus the double period generation number N.

Fibonacci case presented here. Also we can observe that the derivative $d\omega/dk$ is negative, and consequently the group velocity is negative in this region. This result has been observed previously for the periodic magnonic superlattice [16] and it is a consequence of the geometry of the system, i.e., both the applied field and the in-plane k_x wavevector are *perpendicular* to each other. The bandwidth distribution is shown in Fig. 2(c) for a fixed value of the dimensionless wavevector ($kd_A = 0.15$). We can observe that, for large N, the allowed band regions get narrower and narrower, as an indication of more localized modes, as expected. We can also note that the bandwidth distribution presents a typical self-similar Cantor set structure. In fact, this is a usual behavior of quasiperiodic systems [1–3]. More interesting, however, is the plot of the total allowed bandwidth Δ versus the Fibonacci number F_N. This is illustrated in Fig. 2(d) for three different values of kd_A, namely 0.15, 0.25, and 0.35. One can observe that Δ obeys a power law of the form $\Delta \sim F_N^{-\delta}$, and we can conclude from our numerical results that the exponent δ is a function of the common in-plane wavevector kd_A.

The magnon spectra for the fourth generation of the Thue–Morse quasiperiodic sequence is shown in Fig. 3. In Fig. 3(a) it is possible to see that the band gaps are larger for the Thue–Morse case when compared to the Fibonacci one. In fact, the Thue–Morse sequence is considered more disordered than the Fibonacci sequence. Therefore, the higher the disorder of the structure, the narrower the bulk bands [1–3]. The inset shows that, as in the Fibonacci case, the spin wave modes are in two regions. The low-frequency region is in the range 193.3 GHz $< \omega <$ 193.9 GHz, while the high-frequency region is in the range 194.8 GHz $< \omega <$ 273.9 GHz (for zero external applied field and $kd_A = 0$). We can see that the low-frequency region limits are the same for both Fibonacci and Thue–Morse cases. However, for the high-frequency region only the lower band limit is the same. This is because the Thue–Morse bulk band is narrower than the Fibonacci one. We can also observe a narrowing of the regions as the applied magnetic field is increased (see Fig. 3(b)). These results are different from the results for the periodic case for $H_0 = 0$. In fact, they are closer to the double period case described in the next paragraph. The results for $H_0 = 22$ kG, compared to the periodic case, are qualitatively the same, i.e., a narrowing of the allowed frequency regions and the spin wave modes are concentrated in the low-frequency region (see Ref. [16]). Fig. 3(c) shows the forbidden and allowed regions of propagation of the spin waves for the Thue–Morse superlattice. We have again considered the in-plane wavevector $kd_A = 0.15$ and have plotted the regions as a function of the Thue–Morse generation number N. The localization of the bulk bands is clear as N increases. The total allowed bandwidth Δ scales as the power law $\Delta \sim (2^N)^{-\delta}$. This is shown in Fig. 3(d) for $kd_A = 0.15$, 0.25, and 0.35. Our numerical results again show that δ is a function of the common in-plane wavevector kd_A.

Finally, the magnon spectra for the fourth generation of the double period quasiperiodic structure with mirror symmetry is shown in Fig. 4. In Fig. 4(a) it is the dispersion relation for the applied field $H_0 = 0$. The results are similar to those of Fibonacci and Thue–Morse cases: there is a low-frequency region (193.3 GHz $< \omega <$ 193.9 GHz) and there is a high-frequency region (194.8 GHz $< \omega <$ 295.7 GHz). The limits of the allowed regions for the double period case are also the same as that of

Fibonacci and Thue–Morse cases, but the upper limit of the high-frequency region. For the situation in which the applied field is $H_0 = 22$ kG, the spectra present a similar behavior, i.e., the bulk bands get narrower. On the other hand, if we compare these results to the periodic case [16], we can note, as in the Thue–Morse case, a distinct behavior when the applied field goes to zero, and a very similar qualitative result when the applied field corresponds to 22 kG. The forbidden and allowed regions, as a function of the double period generation number N, are shown in Fig. 4(c). One can see that the bandwidth distribution of the Thue–Morse and double period cases are more similar, compared to the Fibonacci case. This is because Thue–Morse and double period sequences are in the same *universality class* [1–3]. The log–log plot of the scaling behavior of the allowed bandwidth, which is $\Delta \sim (2^N)^{-\delta}$ (as in the Thue–Morse case), is shown in Fig. 4(d) for $kd_A = 0.15, 0.25$, and 0.35. Although the number of allowed bands and their scaling behavior are similar to the Thue–Morse case, our numerical results show that the behavior of the exponent δ for the double period sequence is closer to the Fibonacci case. A similar behavior has been reported for ferromagnetic quasiperiodic superlattices [21].

In summary, we have discussed the spectra, localization and scaling laws of spin waves which can propagate in quasiperiodic magnonic structures following the Fibonacci, Thue–Morse and double period sequences. Once the defining rules of these sequences impose long-range correlations, it is plausible to search for global (universal) consequences of these correlations. The global aspects of these sequences were found in their bandwidth structures, which are fractal objects presenting self-similar properties, as exemplified in Fig. 2 for the Fibonacci case and verified also for the other two sequences. Much more interesting, however, are the power laws which govern the scale of the spectra for each sequence (Figs. 2(d), 3(d) and 4(d) for Fibonacci, Thue–Morse and double period sequences, respectively). We found that the scaling index δ depends only upon the particular sequence being tested, and in this way, we can say that they can promptly identity each kind of sequence. The most appropriate experimental technique for studying the spin wave spectra is light scattering spectroscopy of Raman and Brillouin type [13,22]. Surely our model can be realized experimentally and we hope that experimentalists are encouraged to investigate it.

Acknowledgements

This work was partially financed by the Brazilian Research Agency CAPES, CNPq, FINEP and FAPEMA.

References

[1] E.L. Albuquerque, M.G. Cottam, Polaritons in Periodic and Quasiperiodic Structures, Elsevier, Amsterdam, 2004.
[2] E. Maciá, F. Dominguez-Adame, Electrons, Phonons and Excitons in Low Dimensional Aperiodic Systems, Editorial Complutense, Madri, 2000.
[3] E.L. Albuquerque, M.G. Cottam, Phys. Rep. 376 (2003) 225.
[4] M.N. Baibich, J.M. Broto, A. Fert, F.N. Vandau, F. Petroff, P. Eitenne, G. Creuzet, A. Friederich, J. Chazelas, Phys. Rev. Lett. 61 (1988) 2472.
[5] P.F. Carcia, A.D. Meinhaldt, A. Suna, Appl. Phys. Lett. 47 (1985) 178.
[6] A. Saib, D. Vanhoenacker-Janvier, I. Huynen, A. Encinas, L. Piraux, E. Ferain, R. Legras, Appl. Phys. Lett. 83 (2003) 2378.
[7] I.L. Lyubchanskii, N.N. Dadoenkova, M.I. Lyubchanskii, E.A. Shapovalov, T.H. Rasing, J. Phys. D: Appl. Phys. 36 (2003) R277.
[8] J.R. Childress, R.E. Fontana Jr., C. R. Physique 6 (2005) 997.
[9] T. Freire, C. Chesman, C.G. Bezerra, A.B. Oliveira, M. Assolin, Solid State Commun. (submitted for publication).
[10] Y. Narumi, K. Katsumata, Y. Tanaka, T. Nakamura, S. Shimomura, Y. Tabata, S. Kimura, M. Matsuda, Phys. B 346 (2004) 11.
[11] E. Yablonovitch, Phys. Rev. Lett. 58 (1987) 2059.
[12] S. John, Phys. Rev. Lett. 58 (1987) 2486.
[13] D.J. Lockwood, A.H. MacDonald, G.C. Aers, M.W.C. Dharma-wardana, R.L.S. Devine, W.T. Moore, Phys. Rev. B 36 (1987) 9286.
[14] V.V. Kruglyak, A.N. Kuchko, Phys. B 339 (2003) 130.
[15] V.V. Kruglyak, R.J. Hicken, J. Magn. Magn. Matter. 306 (2006) 191.
[16] M.S. Vasconcelos, D.H.A.L. Anselmo, C.G. Bezerra, Solid State Commun. 135 (2005) 673.
[17] R.E. Camley, M.G. Cottam, Phys. Rev. B 35 (1987) 189.
[18] D.H.A.L. Anselmo, M.G. Cottam, E.L. Albuquerque, J. Appl. Phys. 85 (1999) 5774.
[19] M.S. Vasconcelos, E.L. Albuquerque, A.M. Mariz, J. Phys.: Condens. Matter 10 (1998) 5839.
[20] W.B. Yelon, C. Vettier, J. Phys. C 8 (1975) 2760;
G.C. Psaltakis, G. Mischler, D.J. Lockwood, M.G. Cottam, A. Zwick, S. Legrand, J. Phys. C 17 (1984) 1735.
[21] C.G. Bezerra, E.L. Albuquerque, Phys. A 245 (1997) 379;
C.G. Bezerra, M.G. Cottam, Phys. Rev. B 65 (2002) 054412.
[22] P. Grünberg, K. Mika, Phys. Rev. B 27 (1983) 2955.